Detection and Time Course of Formation of Major Thiamin Diphosphate-Bound Covalent Intermediates Derived from a Chromophoric Substrate Analogue on Benzoylformate Decarboxylase[†]

Sumit Chakraborty,[‡] Natalia S. Nemeria,[‡] Anand Balakrishnan,[‡] Gabriel S. Brandt,[§] Malea M. Kneen,[∥] Alejandra Yep,[∥] Michael J. McLeish,[∥,⊥] George L. Kenyon,[∥] Gregory A. Petsko,[§] Dagmar Ringe,[§] and Frank Jordan*[,‡]

Department of Chemistry, Rutgers University, Newark, New Jersey 07102, Department of Medicinal Chemistry, College of Pharmacy, University of Michigan, Ann Arbor, Michigan 48109, and Departments of Chemistry and Biochemistry, Rosenstiel Basic Medical Sciences Research Center, Brandeis University, Waltham, Massachusetts 02454

Received September 22, 2008; Revised Manuscript Received November 10, 2008

ABSTRACT: The mechanism of the enzyme benzoylformate decarboxylase (BFDC), which carries out a typical thiamin diphosphate (ThDP)-dependent nonoxidative decarboxylation reaction, was studied with the chromophoric alternate substrate (*E*)-2-oxo-4(pyridin-3-yl)-3-butenoic acid (3-PKB). Addition of 3-PKB resulted in the appearance of two transient intermediates formed consecutively, the first one to be formed a predecarboxylation ThDP-bound intermediate with λ_{max} at 477 nm, and the second one corresponding to the first postdecarboxylation intermediate the enamine with λ_{max} at 437 nm. The time course of formation/depletion of the PKB−ThDP covalent complex and of the enamine showed that decarboxylation was slower than formation of the PKB−ThDP covalent adduct. When the product of decarboxylation 3-(pyridin-3-yl)acrylaldehyde (PAA) was added to BFDC, again an absorbance with λ_{max} at 473 nm was formed, corresponding to the tetrahedral adduct of PAA with ThDP. Addition of well-formed crystals of BFDC to a solution of PAA resulted in a high resolution (1.34 Å) structure of the BFDC-bound adduct of ThDP with PAA confirming the tetrahedral nature at the C2α atom, rather than of the enamine, and supporting the assignment of the λ_{max} at 473 nm to the PAA−ThDP adduct. The structure of the PAA−ThDP covalent complex is the first example of a product−ThDP adduct on BFDC. Similar studies with 3-PKB indicated that decarboxylation had taken place. Evidence was also obtained for the slow formation of the enamine intermediate when BFDC was incubated with benzaldehyde, the product of the decarboxylation reaction thus confirming its presence on the reaction pathway.

The enzyme benzoylformate decarboxylase (BFDC;[1] EC 4.1.1.7) from *Pseudomonas putida* is an essential component of the mandelate pathway in which mandelic acid is used as a sole carbon source. BFDC is a thiamin diphosphate (ThDP) dependent enzyme and catalyzes the nonoxidative decarboxylation of benzoylformate to benzaldehyde (*1, 2*). According to the accumulated knowledge on ThDP enzymes, a plausible mechanism for BFDC can be written in terms of three ThDP-bound covalent intermediates (*3, 4*) (Scheme 1): the substrate·ThDP adduct or mandelylthiamin diphosphate (MThDP); the product of decarboxylation, the enamine or C2α-carbanion; and the product·ThDP adduct or C2α-hydroxybenzylthiamin diphosphate (HBThDP). Spectroscopic observation of these three intermediates, and determination of the time course of their formation and depletion, including delineation of the rate-limiting steps, poses a challenge to the mechanistic enzymologist. The only intermediate along the pathway that carries π conjugation, hence is potentially observable by electronic spectroscopy, is the enamine. According to model studies at Rutgers, the enamine resulting from decarboxylation of MThDP (or C2α ionization of HBThDP) should have a λ_{max} near 380 nm (*5, 6*), while the λ_{max} values for the aromatic rings in the MThDP and HBThDP intermediates should be lower than 260 nm. This spectral region is overlapped with the protein envelope. However, these intermediates do exist in their 1′,4′-iminopyrimidine tautomeric forms, characterized by an electronic transition in the 300−312 nm region; see below. In the past, we used *p*-nitrobenzoylformate which gave rise to bands in the visible spectrum for both the MThDP analogue and the

[†] Supported by Grants NIH GM050380 (Rutgers) and NSF EF-0425719 (Brandeis, Michigan).

* To whom correspondence should be addressed. E-mail: frjordan@newark.rutgers.edu. Tel: 973-353-5470. Fax: 973-353-1264.

[‡] Rutgers University.

[§] Brandeis University.

[∥] University of Michigan.

[⊥] Present address: Department of Chemistry and Chemical Biology, IUPUI, Indianapolis, IN 46202.

[1] Abbreviations: ThDP, thiamin diphosphate; MThDP, C2α-mandelylThDP, the covalent adduct formed between ThDP and benzoylformate; 3-PKB, (*E*)-2-oxo-4(pyridin-3-yl)but-3-enoic acid; PKB−ThDP, the covalent adduct formed between ThDP and 3-PKB; HBThDP, C2α-hydroxybenzylThDP, the covalent adduct formed between ThDP and benzaldehyde; PAA, (*E*)-3-(pyridin-3-yl)acrylaldehyde; PHB−ThDP, the covalent adduct formed between ThDP and PAA; MAP, acetylphosphonic acid methyl ester sodium salt; BFDC, benzoylformate decarboxylase from *P. putida*; BAL, benzaldehyde lyase from *P. fluorescens*; MPD, 2-methyl-2,4-pentanediol; YPDC, pyruvate decarboxylase from *S. cerevisiae.*

10.1021/bi801810h CCC: $40.75
Published on Web 01/13/2009

Scheme 1: BFDC Mechanism

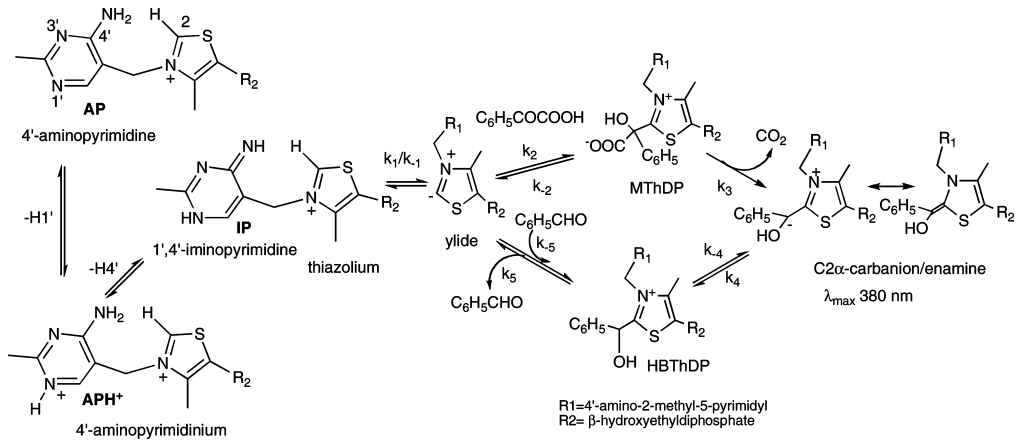

enamine, thereby providing detailed kinetic information about these intermediates on BFDC (*7, 8*).

Recently, a new class of conjugated α-keto acids, (*E*)-2-oxo-4-(pyridin-*x*-yl)but-3-enoic acid (where $x = 2$, 3 or 4), was synthesized at Rutgers and applied to mechanistic studies of wild-type yeast pyruvate decarboxylase (YPDC (*9*)), as well as to YPDC variants created by substitution at the active center (*10*), and at a key mobile loop distant from the active center (*11*). The *meta* isomer (*E*)-2-oxo-4-(pyridin-3-yl)but-3-enoic acid (3-PKB) produced the most informative results (*9*) and enabled (a) observation of an MThDP analogue (PKB−ThDP) and the enamine intermediate; (b) delineation of a pathway for communication between active sites; (c) assignment of specific roles to active site residues of YPDC in the mechanism of catalysis; and (d) delineation of protein-induced chirality of the enamine intermediate.

At the same time, we have started to understand the function of the 4′-aminopyrimidine ring in catalysis by ThDP enzymes, an interest at Rutgers and at Halle, Germany for more than 30 years (*3, 4, 12, 13*). Our progress on this issue was facilitated by the recognition and elucidation of the source of two electronic transitions best detected on enzymes by circular dichroism (CD) methods: (a) a positive band in the 300−312 nm range is associated with the 1′,4′-iminopyrimidine tautomer of ThDP (IP form) seen sometimes even in the absence of substrate (*14*), or in tetrahedral adducts of ThDP with substrate/product (*15*−*19*); (b) a negative band in the 320−330 nm range (attributed to a charge transfer transition between the thiazolium and 4′-aminopyrimidine rings) is associated either (i) with the 4′-aminopyrimidine form (AP form) in the absence of substrate (*14, 19*) or (ii) with a Michaelis complex of ThDP with the substrate pyruvate (*17, 20*) or, in some cases, with a substrate analogue (*14, 17, 21*). CD spectroscopy is the method of choice for monitoring the electronic transitions corresponding to the IP and AP forms since the corresponding CD bands have opposite phases. We have also found that addition of any of the following, sodium methyl acetylphosphonate (MAP), sodium acetylphosphinate or sodium acetylmethylphosphinate, to several pyruvate decarboxylating ThDP enzymes led to formation of the phosphonolactylThDP or phosphinolactylThDP, stable analogues of C2α-lactylThDP (*14, 17, 21*). In some cases the Michaelis complex is detected as well, or solely.

The objective of the present study is to detect, characterize and determine the kinetic fate and spatial orientation of the intermediates in the catalytic cycle of BFDC by using a chromophoric substrate analogue 3-PKB and to gain further insight to the role of the 4′-aminopyrimidine ring of ThDP in catalysis in BFDC, i.e., to assign the state of tautomerization/ionization to each intermediate on the pathway. The chromophoric substrate allows us to study the predecarboxylation, the enamine and the second postdecarboxylation intermediate in solution- information not available from other methods. While there is an NMR method in the literature (*22*) to study the major intermediates on ThDP enzymes by acid quench of the reaction mixture at steady state, the enamine and the second postdecarboxylation intermediate are in protolytic equilibrium and the acid quench converts the enamine to the latter.

The results also provide additional support for the alternative active sites mechanism in BFDC.

Given the attribute of BFDC to form crystals that diffract to high resolution, the structure of the enzyme was solved in the presence of both 3-PKB and the product of its decarboxylation to 3-(pyridin-3-yl)acrylaldehyde (PAA). The structural data support the assignment of the long wavelength visible spectral absorption to a tetrahedral covalent complex formed between the substrate/product and ThDP.

MATERIALS AND METHODS

Benzoylformate, benzaldehyde, (*E*)-3-(pyridin-3-yl)acrylaldehyde (PAA) were purchased from Sigma-Aldrich (St. Louis, MO). All chemicals purchased were of the highest purity grade available and were used without any further purification. Benzaldehyde lyase (BAL) was purified as reported elsewhere (*19*). ^{1}H NMR spectra were recorded on a VARIAN Inova 500 MHz spectrometer.

Synthesis of (E)-2-Oxo-4-(pyridin-3-yl)but-3-enoic Acid (3-PKB). Briefly, the method in ref *23* for synthesis was used. Pyruvic acid ($CH_3COCOOH$, 4.4 g, 50 mmol) was added dropwise to pyridine-3-carbaldehyde (5.35 g, 50 mmol) at 0 °C. Next, KOH (3.5 g, 62.5 mmol) in 20% MeOH (18 mL) was added slowly. The mixture was stirred for 2 h. The crude product was obtained by filtration, then dissolved in water (10 mL), and the solution pH was adjusted to 2.0 with 3 N HCl at 0 °C. The precipitate was filtered and was recrystallized from MeOH providing 79% of pure product (the compound decomposed in hot MeOH). ^{1}H NMR (500 MHz, D_2O-DSS): δ 8.77 (s, 1H, Ar−H), 8.57 (d, 1H, $J = 4.4$ Hz), 8.18 (d, 1H, $J = 8.0$ Hz, Ar−H), 7.73 (d, 1H, $J = 16.5$ Hz,

−C4═C3−H), 7.53 (m, 1H, Ar−H), 7.02 (d, 1H, $J = 16.5$ Hz, H−C4═C3−).

Identification of Reaction Products between BFDC and 3-PKB. The BFDC (1.7 mg in 0.20 mL, concentration of active centers = 142 μM) was incubated with 3-PKB (5 mM) for about 15 h in 50 mM KH_2PO_4 (pH 7.0) containing 2.5 mM $MgSO_4$ and 0.5 mM ThDP at 4 °C. The reaction was quenched by the addition of 200 μL of 12.5% (w/v) trichloroacetic acid in water. Next, 300 μL of D_2O was added, and the reaction mixture was centrifuged for 15 min at 14,000 rpm and filtered through 0.45 μm Gelman Nylon Acrodisc. ^{1}H NMR spectra were recorded using either Watergate or presaturation pulse methods to suppress the water resonances. The reaction products are shown with the NMR assignments in Figure S1 in the Supporting Information and in Results. The reaction mixture was also analyzed by CD in the near UV region at 250−600 nm. No chiral products of a potential carboligase reaction could be detected.

Construction, Expression and Purification of C-Terminally His_6-Tagged BFDC. The gene for C-terminally histidine tagged BFDC was excised from pKKBFD-his (*24*) using *Nco*1 and *Hin*dIII and ligated into the vector pET24d which had been digested with the same two enzymes. The resulting plasmid, pETBFDC, was transformed into BL21(DE3)pLysS chemically competent cells (Promega). Cultures (1 L) were grown in the presence of 10 μg/mL kanamycin and 10 μg/mL chloramphenicol until $OD_{600} \cong 0.8$ and then induced with 1 mM IPTG. After overnight growth at 25 °C, the cells were harvested, resuspended in buffer A (50 mM potassium phosphate buffer pH 8.0, 500 mM NaCl) containing 10 mM imidazole, and disrupted by sonication and cell debris was removed by centrifugation. The cell free extract was applied to a Ni-NTA column connected to a BioLogic LP system (BioRad) and previously equilibrated with the same buffer. The column was washed with buffer A containing 50 mM imidazole, and BFDC was subsequently eluted in buffer A containing 250 mM imidazole. The fractions of highest purity as assessed by SDS−PAGE were pooled, and the buffer was exchanged for a storage buffer (100 mM potassium phosphate buffer pH 6.0, 1 mM $MgSO_4$, 0.5 mM ThDP, 10% glycerol) using Econo-Pac 10 DG desalting columns (BioRad). The protein samples were concentrated with Amicon Ultra centrifugal filters (Millipore), aliquoted and stored at −80 °C.

The purified enzyme ran as a single band on SDS−PAGE. Protein concentrations were determined with the Bradford assay (*25*) using bovine serum albumin as standard.

BFDC Activity Assay. The activity of BFDC was measured using a NADH/horse liver alcohol dehydrogenase (HLADH) coupled assay (*26*). In a typical assay, 1 mL of the reaction mixture contained in 50 mM KH_2PO_4 (pH 6.0): benzoylformate (3.5 mM), $MgSO_4$ (2.5 mM), ThDP (0.5 mM), NADH (0.28 mM) and 0.25 mg (10 units) of HLADH. The reaction was initiated by the addition of 3.1 μg of BFDC. The disappearance of NADH was monitored at 340 nm at 30 °C. The specific activity of BFDC of 345 units·mg protein^{-1} was similar to that reported in the literature (360 units·mg protein^{-1}) (*26*).

Rapid-Scan Stopped-Flow Photodiode Array (PDA) Experiments. These experiments were carried out on an SX.18MV stopped-flow spectrophotometer from Applied Photophysics (Leatherhead, United Kingdom). Experiments were performed by mixing an equal volume of BFDC and substrate/inhibitor of intended concentrations. Typically, 1600 spectra were collected for each experiment with varied reaction times and the lowest time interval of 2.5 ms. A slit width of 2 mm and a path length of 2 mm were used (see specific conditions for each experiment in the figure legends). PDA spectral data were deconvoluted using Pro-Kineticist (Pro/K) Global kinetic analysis software version 4.21 from Applied Photophysics. In each deconvolution, singular value decomposition (SVD) of data sets was determined using Pro/K which yielded unbiased information about the minimum complexity of the chemical system, independent of model and indicating the number of independent components present. The SVDs generated in this manner were treated using the analysis tool of the same software to fit to a minimally complex model. The convergence was tested with the maximum number of iterations allowed by the software. The model validity was crosschecked using parameter minimization. The fit spectra obtained in this manner were crosschecked by analyzing the raw data sets using PeakFit version 9.0 from Systat. Sigma plot 2001 version 7.101 was used to create the difference spectra and for data analysis.

Circular Dichroism. CD studies were performed on a Chirascan CD spectrometer from Applied Photophysics in a 1 cm path length cell in the near-UV region (as specified in each figure). PAA (1 mM) was added to BFDC (2.0 mg/mL, concentration of active centers 35.5 μM in 20 mM KH_2PO_4 (pH 7.0)) containing ThDP (0.50 mM) and $MgCl_2$ (2.50 mM), and spectra were recorded after 5, 10, 15, 20, 25 and 30 min at 5 °C. PAA (5−50 μM) was also added to benzaldehyde lyase (BAL; 2.0 mg/mL, concentration of active centers 33.9 μM) in 50 mM Tris HCl (pH 7.5) containing ThDP (0.25 mM) and $MgCl_2$ (1.0 mM). Spectra were recorded in the near-UV region at 5 °C. As a control, the spectrum of PAA (100−1000 μM) in 20 mM KH_2PO_4 (pH 7.0) was recorded in the absence and in the presence of 0.10 mM DCPIP. Neither spectrum exhibited any CD signal.

Stopped-Flow CD Experiments. These experiments were carried out on a π*-180 CDF Spectrometer from Applied Photophysics. In a typical experiment, BFDC (83 μM active-site concentration) in 50 mM KH_2PO_4 (pH 6.0) containing 2.5 mM $MgSO_4$ and 0.5 mM ThDP (buffer B) was mixed with an equal volume of 3-PKB of intended concentration in the same buffer. The reaction was monitored for varied time (0.01−200 s), and data points were collected at varied time intervals (2.5−10 ms). A slit width of 2 mm and a path length of 10 mm were used. The temperature was maintained at 30 °C. The data were also analyzed using Pro-K and SVDs were determined where necessary. SigmaPlot 2001 version 7.101 was used for data analysis.

Crystallization of BFDC. Purified BFDC was crystallized as previously described (*1*). Briefly, the protein was concentrated to 30−40 mg/mL in a buffer containing 100 mM potassium phosphate buffer pH 6.0, 1 mM $MgSO_4$, 0.5 mM ThDP and 10% glycerol. A well solution containing 100 mM TrisHCl (pH 8.5), 150 mM $CaCl_2$, 0.5% (v/v) MPD [2-methyl-2,4-pentanediol], and 22% (v/v) PEG 400 was mixed with the protein in a ratio of 2:5 or 3:4 and equilibrated by hanging drop vapor diffusion. Large, well-formed crystals appeared within five days. Crystals were transferred to a cryoprotecting formulation of the well solution containing 30% glycerol (v/v) and 2 mM 3-PKB or PAA dissolved in DMSO (final

Table 1: Crystallographic Statistics for Structures of BFDC with PAA and 3-PKB

data set	BFDC with PAA	BFDC with 3-PKB
PDB ID code	3F6B	3F6E
beamline	APS, GM/CA-CAT, 23-ID-D	APS, GM/CA-CAT, 23-ID-D
wavelength (Å)	1.0332	1.0332
space group	I_{222}	I_{222}
unit cell	$a = 81.5$, $b = 96.1$, $c = 137.4$	$a = 81.1$, $b = 95.8$, $c = 137.3$
resolution limits	50.0−1.34 (1.39−1.34)	50.0−1.44 (1.51−1.44)
total reflections	120075	119545
unique reflections	114739	98827
% completeness (last shell)	95.7 (85.1)	82.8 (82.0)
redundancy (last shell)	5.9 (3.8)	4.5 (3.7)
$I/\sigma(I)$	16.9 (1.89)	11.9 (2.14)
R_{merge}	0.089 (0.61)	0.11 (0.49)
unit cell contents		
molecules/ASU	1	1
solvent content (%)	48.6	48.1
refinement statistics		
resolution range (Å)	50.0−1.34	50.0−1.44
R_{work} (%)	17.9	19.6
R_{free} (%)	19.8	21.9
no. of residues	523	523
no. of waters	431	373
average B factor (Å^2)	16.3	15.7
rmsd		
bond lengths (Å)	0.01	0.02
bond angles (deg)	1.43	1.74
Ramachandran analysis		
most favored (%)	98.66	98.27
allowed (%)	100	100

DMSO concentration, 2% v/v). A pronounced yellowish color developed within the crystals within seconds of addition to the 3-PKB or PAA solutions.

Data Collection and Processing. Diffraction data were obtained from the beamline 23-ID-D, administered by GM/CA-CAT, at the Advanced Photon Source (APS, Argonne National Laboratories). Data were processed as described previously, using both the CCP4 and Phenix suite of crystallographic software programs. Crystals diffracted to a spatial resolution of 1.34 Å (PAA) and 1.44 Å (3-PKB). Statistics relevant to data collection and processing were carried out as in ref (*27*), and the results are found in Table 1. The structures have been deposited as PDB entries 3F6B (for PAA) and 3F6E (for 3-PKB).

RESULTS

Identification of ThDP-Bound Intermediates on BFDC Derived from (E)-2-Oxo-4-(pyridin-3-yl)but-3-enoic Acid and (E)-3-(Pyridin-3-yl)acrylaldehyde. (a) Characterization of the Products of the Reaction between BFDC and 3-PKB. According to the accepted mechanism, decarboxylation of 3-PKB by BFDC may lead to two products resulting from protonation at either the C2α or C2γ positions (Scheme 2). The ^{1}H NMR results indicate that the reaction proceeds exclusively through protonation at the C2α position resulting in the formation of PAA. However, during the ^{1}H NMR detection of the products (Figure S1 in Supporting Information), it became apparent that there was an additional compound being formed, which, on comparison with authentic material, turned out to be 3-(3-pyridyl)acrylic acid. Mechanistically, this was not unanticipated since the carbocyclic analogues of 3-PKB also showed this oxidation product (*31*), presumably derived from oxidation of the enamine by O_2.

Using a large concentration of BFDC, quantitative conversion of 3-PKB to PAA (40%) and (*E*)-3-(3-pyridyl)acrylic acid (60%) resulted, and no evidence from either ^{1}H NMR or CD was observed for formation of the expected carboli-

Scheme 2: Alternative Products Resulting from Protonation and Oxidation of the Enamine Derived from 3-PKB

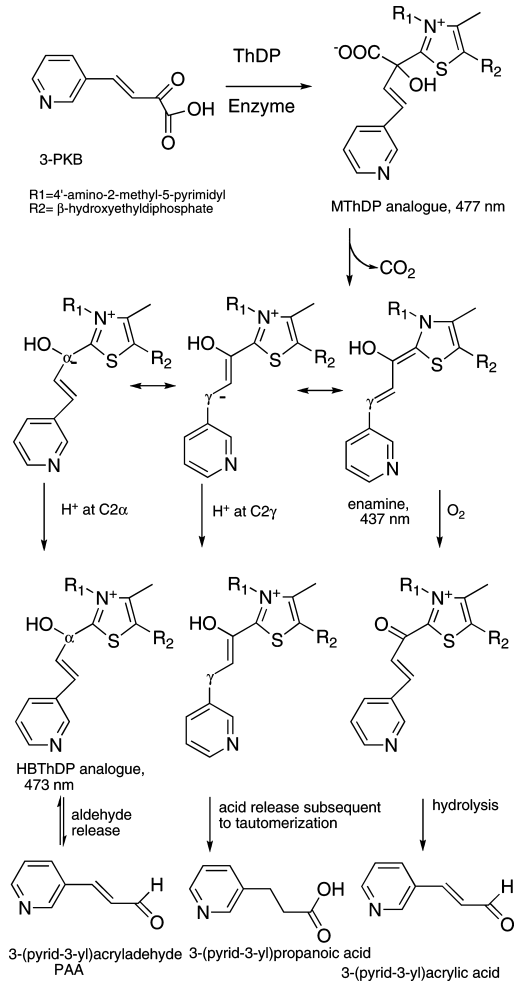

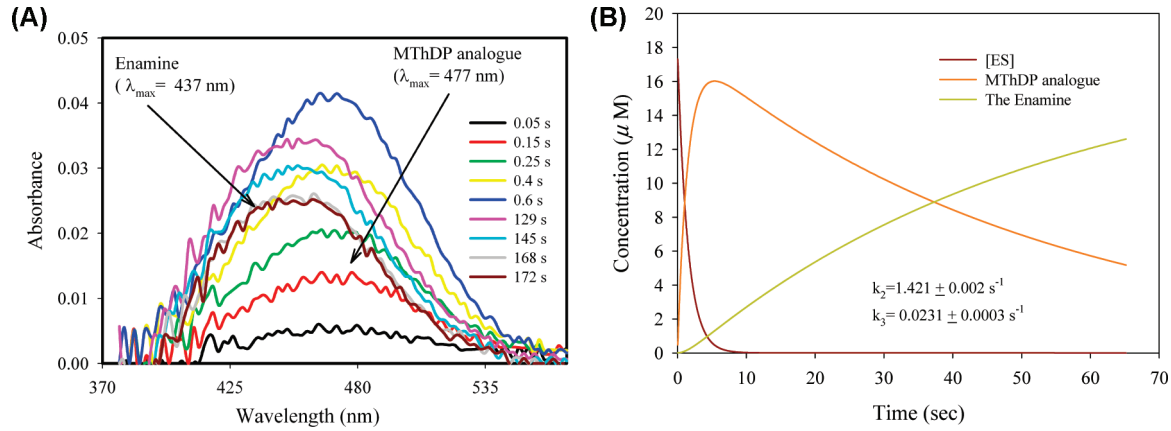

FIGURE 1: Reaction of BFDC with 3-PKB. (A) Difference spectra showing formation of transients in the reaction between BFDC and 3-PKB. BFDC (33.2 μM active-site concentration) in buffer B (see Materials and Methods) was mixed with an equal volume of 10 mM 3-PKB in the same buffer at 30 °C. The reaction was monitored in the wavelength range of 300−595 nm for 264 s, and the spectra were recorded every 5 ms. (B) Time course of formation of MThDP analogue (PKB−ThDP) and the enamine. Difference spectra of the reaction between BFD and PKB were deconvoluted using Pro-Kineticist Global kinetic analysis software version 4.21 according to the model [ES] > [I_1] > [I_2]; initial concentration of [ES] was estimated to be equal to the active-site concentration assuming all sites are occupied.

Scheme 3: Kinetic Constants Determined for ThDP-Bound Intermediates Derived from 3-PKB and PAA

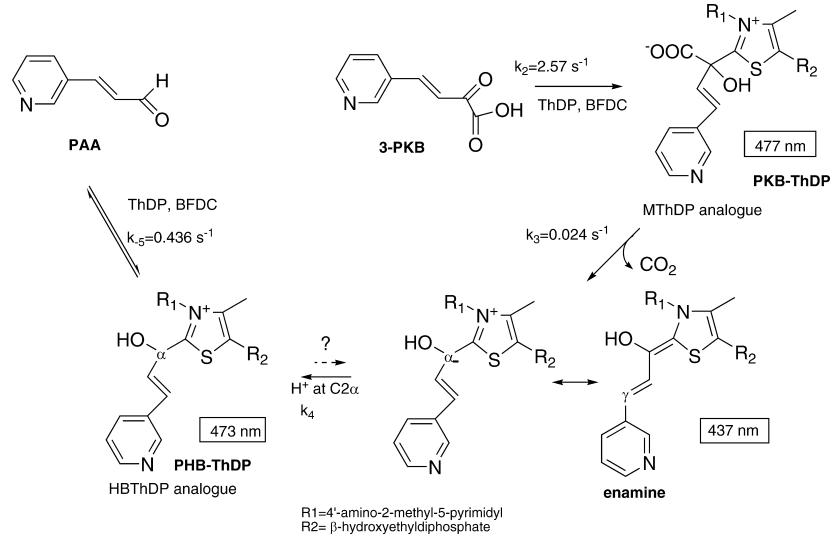

gase product. The chemical shifts were recorded for the two compounds under the acid quench conditions. (*E*)-3-(pyridin-3-yl)acrylaldehyde (3-PAA): ^{1}H NMR (500 MHz, H_2O/D_2O) δ 9.852 (d, J = 7.5 Hz, 1H), 9.227 (s, 1H), 9.016 (d, J = 8.5 Hz, 1H), 8.964 (d, J = 6 Hz, 1H), 8.294 (t, J = 7 Hz, 1H), 8.003 (d, J = 16 Hz, 1H), 7.175 (dd, J = 16 Hz, 7 Hz, 1H). (*E*)-3-(pyridin-3-yl)acrylic acid: ^{1}H NMR (500 MHz, H_2O/D_2O) δ 9.144 (s, 1H), 8.960 (d, J = 8 Hz, 1H), 8.917 (d, J = 5.5 Hz, 1H), 8.253 (t, J = 7 Hz, 1H), 7.926 (d, J = 16 Hz, 1H), 6.948 (d, J = 16 Hz, 1H).

In addition, as observed with the carbocyclic analogues of 3-PKB interacting with YPDC (*28*−*31*), there is significant product inhibition, making steady-state kinetic measurements nearly impossible. Hence, we relied on pre-steady state methods. Since the inhibition is at a much slower time scale than the stopped-flow kinetic studies, the inhibition has no impact on the stopped-flow results and interpretation. Given that on the stopped-flow time scale the enamine appears to be the end product, its subsequent partition to PAA and 3-(3-pyridyl)acrylic acid should not affect the kinetic constants leading to enamine formation.

(b) Stopped-Flow PDA Studies of the Interaction of BFDC with 3-PKB. Difference spectra resulting from the reaction between BFDC and 3-PKB are shown in Figure 1. A first transient (T_1) started to appear with a λ_{max} at 477 nm, reached the maximum and was slowly converted to a second transient (T_2) with a λ_{max} at 437 nm, while the first transient was depleted (Figure 1A). In one individual experiment, the rate constant for the depletion of T_1 was found to be 0.0189 ± 0.0003 s^{-1}, similar to the value of 0.0193 ± 0.0001 s^{-1} observed for the appearance of T_2 (data not shown). Compared with similar bands observed on the reaction of 3-PKB with both YPDC (*9*−*11*) and BAL (*32*), the absorbance at λ_{max} of 477 nm could be assigned to PKB−ThDP, an analogue of MThDP (formed by the reaction between BFDC and benzoylformate), while the absorbance at 437 nm could be assigned to the enamine (Figure 1A, Schemes 2 and 3). The difference spectra were deconvoluted according to the method described in Materials and Methods, and rate constants for PKB−ThDP and enamine formation of 1.421 s^{-1} and 0.0231 s^{-1}, respectively, were calculated as shown in Figure 1B. These indicated that decarboxylation was slower than PKB−ThDP formation. Next, it was demonstrated that the rate constant for the PKB−ThDP formation is substrate concentration dependent, increasing with increas-

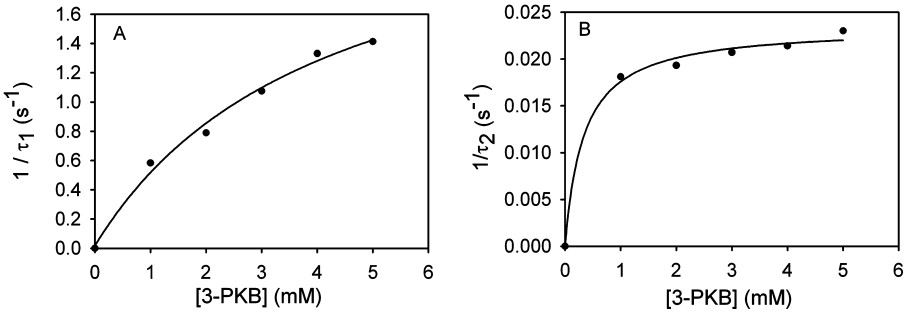

FIGURE 2: Dependence of the rate of formation of 3-PKB−ThDP and enamine on the concentration of 3-PKB. (A) Concentration dependence of the PKB−ThDP formation. BFDC (concentration of active centers 33.2 μM) in buffer B was mixed with an equal volume of 2, 4, 6, 8, and 10 mM 3-PKB in the same buffer at 30 °C. The reaction was monitored in the 300−595 nm wavelength range for 264 s. (B) Concentration dependence of enamine formation. Conditions as in A. Solid lines represent the best fit of $1/\tau_1$ vs [3-PKB] and $1/\tau_2$ vs [3-PKB] according to the equations $1/\tau_1 = k_2[\text{3-PKB}]/(K_{d1} + [\text{3-PKB}]) + k_{-2}$ and $1/\tau_2 = k_3[\text{3-PKB}]/(K_{d2} + [\text{3-PKB}])$, respectively.

ing 3-PKB concentration (Figure 2A); unexpectedly, so did the rate constant of enamine formation (Figure 2B).

Relaxation kinetic theory (*33*) was used to treat and interpret the transient kinetic data. The formation of the PKB−ThDP in Scheme 2 is described by the τ_1 relaxation, and the formation of enamine is described by the τ_2 relaxation. As shown in Figures 2A and 2B, the substrate concentration dependence of both $1/\tau_1$ and $1/\tau_2$ is curved for the reaction with 3-PKB. The deduced rate constants (see legend to Figure 2 for equations used) for PKB−ThDP formation were k_2 =2.57 ± 0.42 s^{-1} and k_{-2} is essentially zero within the experimental error. The rate constant of enamine formation was $k_3 = 0.024 \pm 0.001$ s^{-1}, confirming that the decarboxylation of PKB−ThDP is much slower than its formation. Values of $K_{d1} = 4.14 \pm 1.4$ mM for 3-PKB binding in the first active center and $K_{d2} = 0.34$ mM for its binding in the second active center were also obtained, clearly indicative of positive cooperativity of active centers on 3-PKB binding. The rate constants for PKB−ThDP and enamine formation from this treatment (2.57 and 0.024 s^{-1}) were in good agreement with those obtained from deconvolution of the PDA data (Figure 1).

(c) Stopped-Flow CD Studies of BFDC with 3-PKB Confirmed the Formation of Two Transient Intermediates. The reaction between 3-PKB and BFDC also was monitored on a stopped-flow CD spectrometer at 435 nm (this instrument must be used at a single wavelength unlike the PDA on the stopped-flow absorbance instrument). Initially, a negative ellipticity started to develop which persisted for the first 6 s. This was followed by the formation of positive ellipticity with an exponential rise to maximum (Figure 3). A comparison with the stopped-flow PDA studies, and observations with 3-PKB on YPDC (*9*−*11*), suggested that the negative ellipticity corresponds to the PKB−ThDP, and the positive one to the enamine (Figure 3). The time course at 435 nm has a contribution from the band at 437 nm (positive ellipticity) and the band at 477 nm (negative ellipticity). The rate constant for enamine formation was 0.0226 s^{-1}. Within experimental error this was similar to that determined in the stopped-flow PDA experiment (0.0231 s^{-1}), and to that calculated from the substrate concentration dependence in the paragraph above (0.024 s^{-1}).

(d) Stopped-Flow PDA Studies of BFDC with PAA Revealed Formation of the PAA−ThDP Adduct. When BFDC was reacted with 3-PKB, two transients were detected (the PKB−ThDP adduct and the enamine) but the HBThDP analogue, PHB−ThDP (Scheme 3), was not observed.

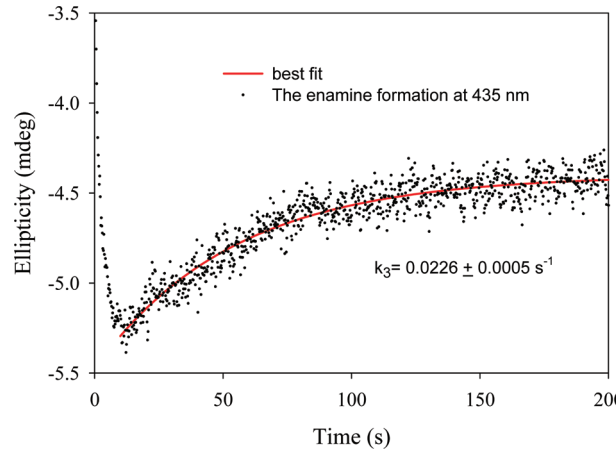

FIGURE 3: Reaction of BFDC with 3-PKB monitored by stopped-flow CD. BFDC (33.2 μM) in buffer B was mixed on a stopped-flow CD with an equal volume of 10 mM 3-PKB in the same buffer at 30 °C. The reaction was monitored for 200 s at 435 nm with a path length of 1 cm and slit width of 2 nm. 5000 data points were collected at 0.012 s interval.

Earlier, when 3-PKB was used with YPDC and its variants (*9*−*11*), no evidence was found for formation of the HEThDP/HBThDP analogue, though ^{1}H NMR studies enabled observation of this intermediate in the steady state (*11*). Stopped-flow studies were also carried out with BFDC and PAA to investigate whether PHB−ThDP, and the enamine could be formed starting from the product of the 3-PKB reaction. This addresses the question of reversibility of the last two steps in Scheme 1, i.e., the addition of aldehyde to form the HBThDP, perhaps followed by deprotonation at the C2α position forming the enamine. Mixing PAA and BFDC produced a broad charge transfer band with λ_{max} = 473 nm (Figure 4A). The band persisted for 5 min, and no sign of its conversion to any other band could be detected. We propose that this band corresponds to the formation of the tetrahedral intermediate, PHB−ThDP, with its formation exhibiting an exponential rise to maximum at 473 nm within 7.3 s, with a rate constant of 0.436 ± 0.012 s^{-1} (Figure 4B, Scheme 3).

(e) Interaction of BFDC and BAL with PAA by CD. To gain better understanding of the origins of the visible absorption band near 480 nm on addition of 3-PKB to BFDC, additional CD experiments were carried out. Early CD studies of the BFDC−ThDP complex revealed the presence of the AP form of ThDP (λ_{max} at 323 nm) at higher pH {pK_a = 7.54 for the ([AP] + [IP])/[APH^+] dissociation} (*19*). On

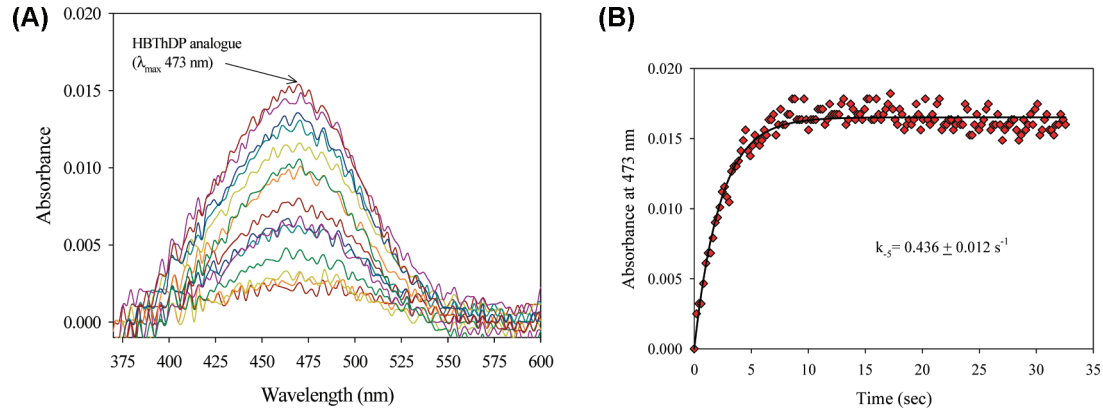

FIGURE 4: Reaction of BFDC with PAA monitored by stopped-flow PDA. (A) Difference spectra showing PHB−ThDP formation in the reaction between BFDC and PAA. BFDC (33.2 μM active-site concentration) in buffer B was mixed with an equal volume of 20 mM PAA in the same buffer at 30 °C. The reaction was monitored in the indicated wavelength range for 32 s, and spectra were recorded every 5 ms. (B) Rate of formation of PHB−ThDP. Reaction conditions as in A. Data were fitted to a single exponential: $A = A_0(1 - \exp(-kt))$ with SigmaPlot vs 7.01. The rate constant k_{-5} refers to that in Scheme 1.

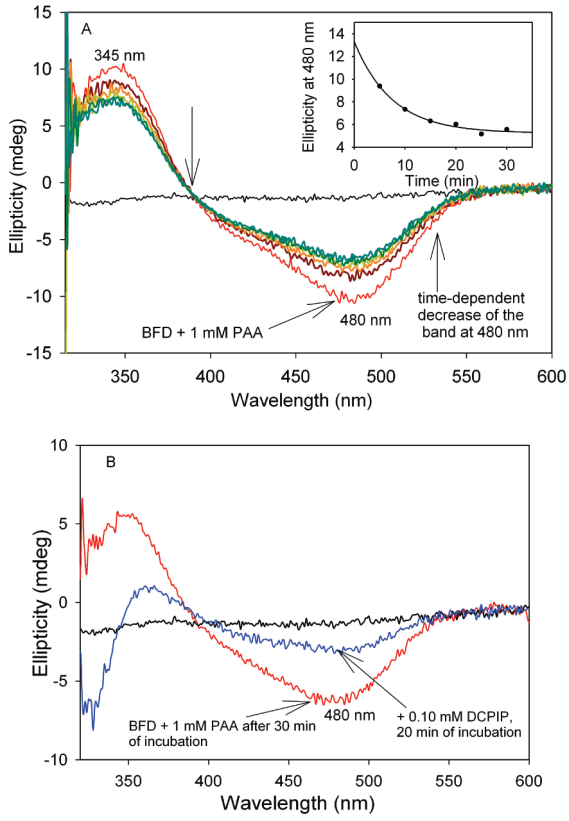

FIGURE 5: CD titration of BFDC by PAA. (A) To BFDC (2.0 mg/mL, concentration of active centers = 35.5 μM) in 20 mM KH_2PO_4 (pH 7.0) containing ThDP (0.5 mM) and $MgCl_2$ (2.5 mM) the PAA (1.0 mM) was added. Spectra were recorded at 5, 10, 15, 20, 25 and 30 min. Inset: time dependent decrease of the CD band at 480 nm. (B) The effect of DCPIP (0.1 mM) addition on the intensity of the band at 480 nm.

addition of PAA (1 mM) to the BFDC·ThDP complex at pH 7.0 and 5 °C, a broad negative band with maximum near 480 nm was observed (Figure 5A). This band was not stable and decreased with time (k_{app} = 0.134 ± 0.03 min^{-1}), reaching steady state level after 30 min (Figure 5, inset), perhaps indicating slow formation of the enamine (Scheme 3, reverse reaction from PHB−ThDP to the enamine). According to our recent studies on BAL with 3-PKB (*32*), the 480 nm band can be assigned to PHB−ThDP on BFDC. If the enamine is indeed formed from PAA, the CD band at 480 nm should be reduced on addition of DCPIP, with the premise that only the enamine among the three ThDP-bound intermediates should be subject to oxidation by DCPIP. Indeed, Figure 5B shows that on addition of DCPIP (0.1 mM) to the sample in Figure 5A, the amplitude of the CD band at 480 nm was significantly reduced suggesting that both PHB−ThDP and the enamine could be formed. In a control experiment it was shown that, in the absence of BFDC, the PAA itself (0.1−1 mM), or with added DCPIP (0.1 mM), no bands are observed in this wavelength region (data not presented).

For comparison, these CD experiments were repeated using BAL. In the absence of PAA, the CD spectrum of the BAL·ThDP complex in the 290−600 nm range displayed a negative band at 326 nm, assigned earlier to the AP form of ThDP (*27*). On titration of BAL with PAA (1−50 μM and 200 μM) the amplitude of the band at 326 nm was significantly reduced and probably three new bands developed: a negative band at 474 nm and a positive one at 310−311 nm, as well as a rather broad and featureless band at 350−450 nm. The amplitude of all bands increased with increasing PAA concentration and displayed saturation with $S_{0.5,\ PAA}$ = 21.4 μM at 310−311 nm and 21.8 μM at 474 nm (Figure 6A inset, data in figure legend), almost certainly suggesting the same species being monitored at 310−311 and 474 nm. On the basis of studies on eight ThDP enzymes, the band at 310−311 nm could be assigned to the 1′,4′ imino tautomer of the PHB−ThDP. On the basis of similar experiments on BAL with 3-PKB (*32*), the negative band at 474 nm could be assigned to the PHB−ThDP. The negative CD band near 480 nm observed on addition of PAA to BFDC could consequently also be assigned to PHB−ThDP which, more likely, exists in equilibrium with the C2α-carbanion/enamine [rate constant of >6 s^{-1} for enamine formation from the less acidic HEThDP (*34*)].

The broad featureless band at 350−450 nm very likely masks the enamine band (λ_{max} for the enamine is 437 nm in PDA spectra in Figure 1), which on these CD spectra is ill resolved. Yet, the band is created simultaneously with the 310−311 and 474 nm bands. This suggests that, on BAL, there is a rapid equilibrium established between the PHB−ThDP and the enamine (Scheme 3). To obtain evidence for this hypothesized rapid equilibrium on BAL,

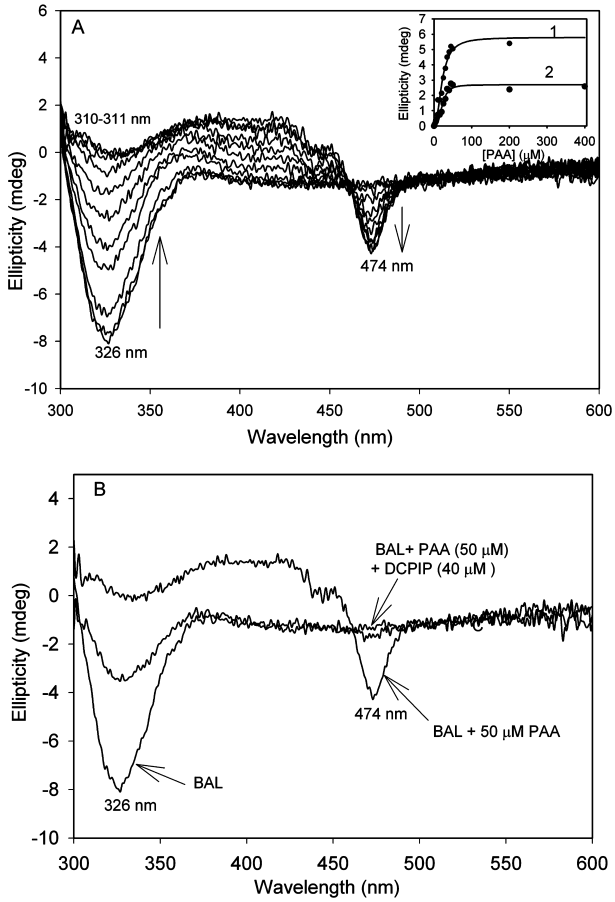

FIGURE 6: CD titration of BAL by PAA. (A) Titration of BAL by PAA. BAL (2.0 mg/mL, concentration of active centers = 33.9 μM) in 50 mM Tris HCl (pH 7.5) containing $MgCl_2$ (1.0 mM) and ThDP (0.25 mM) was titrated by PAA (1−50 μM and 200 μM, 400 μM). The inset shows the dependence of the CD bands at 310−311 nm (1) and at 474 nm (2) on the concentration of PAA. The data were fitted using the Hill equation. Calculated values of $S_{0.5\ PAA}$ were 21.42 ± 1.98 μM (CD band at 310−311 nm) and 21.78 ± 1.92 μM (CD band at 474 nm). (B) Effect of added DCPIP on CD spectra of BAL titrated by PAA. Experimental conditions were as in A.

we carried out an experiment to test the effect of the oxidizing agent DCPIP once more. Addition of DCPIP to the mixture of PAA and BAL in Figure 6A, resulted in simultaneous quenching of all three bands generated in 6A, and reappearance of the band for the AP form of ThDP (Figure 6B). We believe that this is indeed evidence for the presence of the PHB−ThDP ↔ enamine equilibrium.

(f) Stopped-Flow PDA Studies of BFDC with Benzaldehyde Reveal Formation of the Enamine. Apparently, the reaction of PAA with BFDC leads to the formation of the tetrahedral adduct, the PHB−ThDP (Schemes 2 and 3), which may proceed to the enamine, for which the C2α proton would have to be abstracted according to the results in the previous paragraphs. The C2α proton in the PHB−ThDP adduct derived from PAA and BFDC is an allylic proton whereas in the decarboxylation of benzoylformate this proton is benzylic. The pK_as of allylic and benzylic protons are quite different, thus the PHB−ThDP may not reveal enamine formation, and as suggested by the results in Figures 5 and 6, the results may vary with the particular enzyme (Scheme 4). Our ability to demonstrate that PAA is a substrate for BFDC encouraged us to also examine the reaction of BFDC

Scheme 4: Lower Acidity of C2α-Proton in PHB−ThDP than in HBThDP Suggested by the Results on BFDC[a]

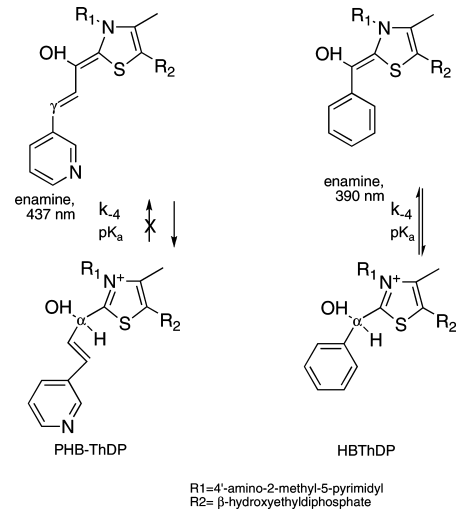

[a] The rationale is based on the evidence that enamine could be produced from benzaldehyde but not from PAA.

in the reverse reaction starting with the true product benzaldehyde.

Reaction of benzaldehyde with BFDC in a stopped-flow PDA instrument led to slow formation of an absorbance band at 393 nm (Figure 7A). This band was not converted to any other band and appeared to be stable for approximately 10 min. Comparing the result with the model studies (*5, 6*), this band could be assigned to the true enamine intermediate (λ_{max} 383 nm in models). The progress curve of enamine formation had an initial lag phase of approximately 100 s, and the data were fitted to a model with two reactive forms of the enzyme: E_1 with one substrate-binding site filled, and E_2 with both substrate-binding sites of the functional dimer filled, and a slow interconversion rate between E_1 and E_2. As outlined in Figure 7B legend, the model led to rates $v_1 = 0.91 \times 10^{-5}$ $\Delta A \cdot s^{-1}$ and $v_2 = 4.32 \times 10^{-5}$ $\Delta A \cdot s^{-1}$ for the two enzyme states, and a rate constant of $k = 0.011$ s^{-1} for the interconversion of the two enzyme states. The analysis clearly shows positive cooperativity with a nearly 5-fold increase in rate, in accord with the alternating sites reactivity proposed for this enzyme (Scheme 5).

Structural Characterization of Intermediates. (a) Observation of Active Site Electron Density for BFDC Reacted with PAA and 3-PKB. To further confirm formation of covalent intermediates between 3-PKB or PAA with ThDP, the BFDC crystals were exposed to each compound separately. Exposure of BFDC to both 3-PKB and PAA gave rise to clear electron density in the vicinity of the ThDP cofactor (Figure 8a,b). Crystals of BFDC incubated with PAA gave rise to electron density suggestive of a covalent link between the PAA aldehyde carbon and the C2 atom of the thiazolium ring of the ThDP cofactor (Figure 8a). By contrast, BFDC crystals soaked with 3-PKB gave no evidence for strong electron density between the keto carbon atom and the thiazolium C2 carbon but did suggest loss of the carboxyl group (Figure 8b). The best fit of the PAA reaction product to the observed electron density yields a structure that is superimposable upon that seen for cocrystallization of BFDC with PAA.

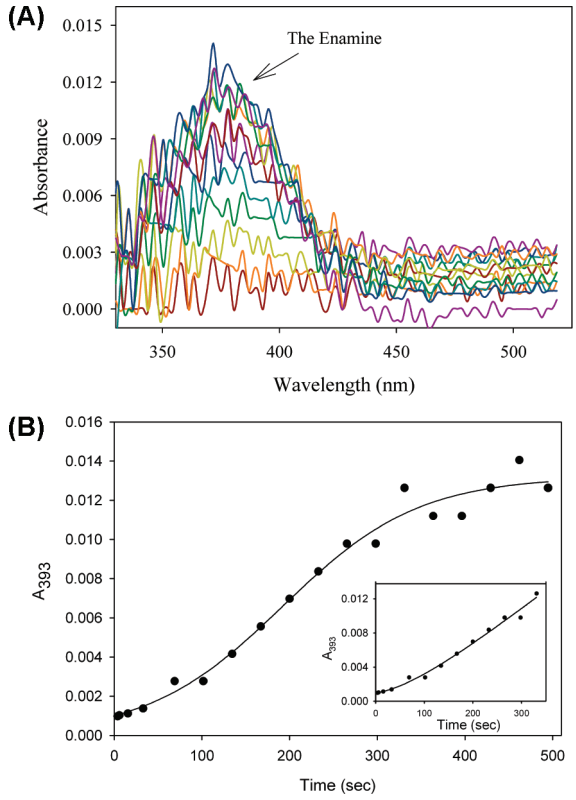

FIGURE 7: Reaction of BFDC with benzaldehyde monitored by stopped-flow PDA. (A) Difference spectra showing enamine formation from benzaldehyde. BFDC (33.3 μM concentration of active centers) in buffer B was mixed with an equal volume of 20 mM benzaldehyde in the same buffer at 30 °C. Reaction was monitored in the 300−595 nm wavelength range for 264 s, and spectra were recorded every 5 ms. (B) Rate of the enamine formation from benzaldehyde at 393 nm. Inset: Progress curve of enamine formation from benzaldehyde in the first 331 s. Data were fitted according to an equation for two enzyme states: $P = y_0 + ((v_1 - v_2)/k)(1 - e^{-kt}) + v_2t$, where v_1 and v_2 depict changes in A_{393} ($\Delta A \cdot s^{-1}$) of two distinct enzyme states E_1 and E_2. The rate constant k pertains to the transition from E_1 to E_2. The values of the parameters are $v_1 = 0.91 \times 10^{-5}$ $\Delta A \cdot s^{-1}$, $v_2 = 4.32 \times 10^{-5}$ $\Delta A \cdot s^{-1}$, $y_0 = 0.001$ and $k = 0.011$ s^{-1}.

Scheme 5: Two Active Forms of the Functional Dimer of BFDC Suggested by Data in Figure 7

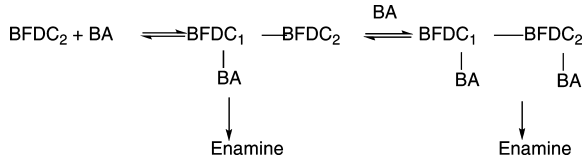

(b) Binding Mode of PHB−ThDP. The residues that interact with the PHB−ThDP and possibly contribute to its stabilization may be seen in Figure 8c. Potential hydrogen bonds to the main and side chains of Ser26 and with an ordered solvent molecule are indicated.

DISCUSSION

Addition of 3-PKB and PAA Enables Detection of All ThDP-Bound Covalent Intermediates. (a) Identification of Intermediates in the Reaction between BFDC and 3-PKB. The stopped-flow PDA studies of the reaction between 3-PKB and BFDC yielded results, which parallel those obtained with YPDC (*9*−*11*) and BAL (*32*). A broad absorbance at λ_{max} 477 nm was formed immediately, which on decaying was converted to another band at λ_{max} 437 nm. The rate of disappearance of the band at λ_{max} 477 nm was found to be equal to the rate of formation of the second band with λ_{max} 437 nm within the experimental error. On the basis of the evidence on three enzymes and some variants of YPDC as well, we have suggested that the bands pertain to the PKB−ThDP (λ_{max} 477 nm) and the enamine (λ_{max} 437 nm, Scheme 3).

(b) Observation of the PHB−ThDP Intermediate in the Reaction of BFDC and PAA. When PAA, the aldehyde product of the decarboxylation of 3-PKB, was reacted with BFDC in the stopped-flow PDA instrument, a broad absorption band was formed at λ_{max} 473 nm. This band is very similar both in shape and in λ_{max} to the charge transfer band we suggested for PKB−ThDP. Formation of this band was complete within 10 s with a rate of constant of 0.436 s^{-1}, and the band persisted for 15 min. A similar band was also observed when PAA was reacted with BAL (*32*). We assign the band to the PHB−ThDP (Scheme 3).

The data suggest that, on BFDC, the C2α-proton on PHB−ThDP is less acidic than the corresponding proton in HBThDP (Scheme 4). This would account for the apparent stability of PHB−ThDP derived from PAA, as when benzaldehyde was used as a substrate the enamine could indeed be observed (see Scheme 4 for a plausible explanation; Figure 7).

Comparison of BFDC and BAL in their ability to convert PHB−ThDP provides additional insight. Apparently, the BAL active center lowers the pK_a at C2α (increases the acidity) more than BFDC for PHB−ThDP, since on BAL there is a broad featureless CD band at 350−450 nm appearing simultaneously with bands attributed to formation of PHB−ThDP (Figure 6A), not seen with BFDC (Figure 5A). Almost certainly, with BAL, the additional CD band at 350−450 nm has the correct phase to encompass the band pertinent to the enamine.

On addition of DCPIP to a mixture of BAL and PAA, we could also determine the relative rates at which the PHB−ThDP is converted to the enamine on the two enzymes. Addition of DCPIP to BAL with PAA resulted in the simultaneous quenching of the three CD features (310−311 nm, 474 nm and the broad feature at 350−450 nm), i.e., the enamine was present as soon as PAA was added to the enzyme (Figure 6B). A similar experiment carried out with BFDC failed to show the broad CD band at 350−450 nm, and once the 480 nm band developed, addition of DCPIP quenched only part of the latter CD band, suggesting that enamine formation in this case from PHB−ThDP was slower than oxidation of enamine by DCPIP (Figures 5A and 5B).

In summary, the enzyme BAL not only increases the acidity more than BFDC at C2α (thermodynamic effect) but it also increases the rate constant k_{-4} for formation of the enamine (Scheme 1). The notion that BAL has a more hydrophobic active site than BFDC is also apparent from the finding that the IP tautomer derived from a stable MThDP analogue has a λ_{max} value of 299 nm for BFDC (in preparation) and 312 nm for BAL (*27*), consistent with models for IP tautomer indicating that lower dielectric constant solvent shift the λ_{max} to longer wavelength (*18*).

(c) Assignment of the Transient Absorbance at 437 nm to the Enamine. Some years ago, there was a synthetic model constructed for the enamine with λ_{max} essentially identical

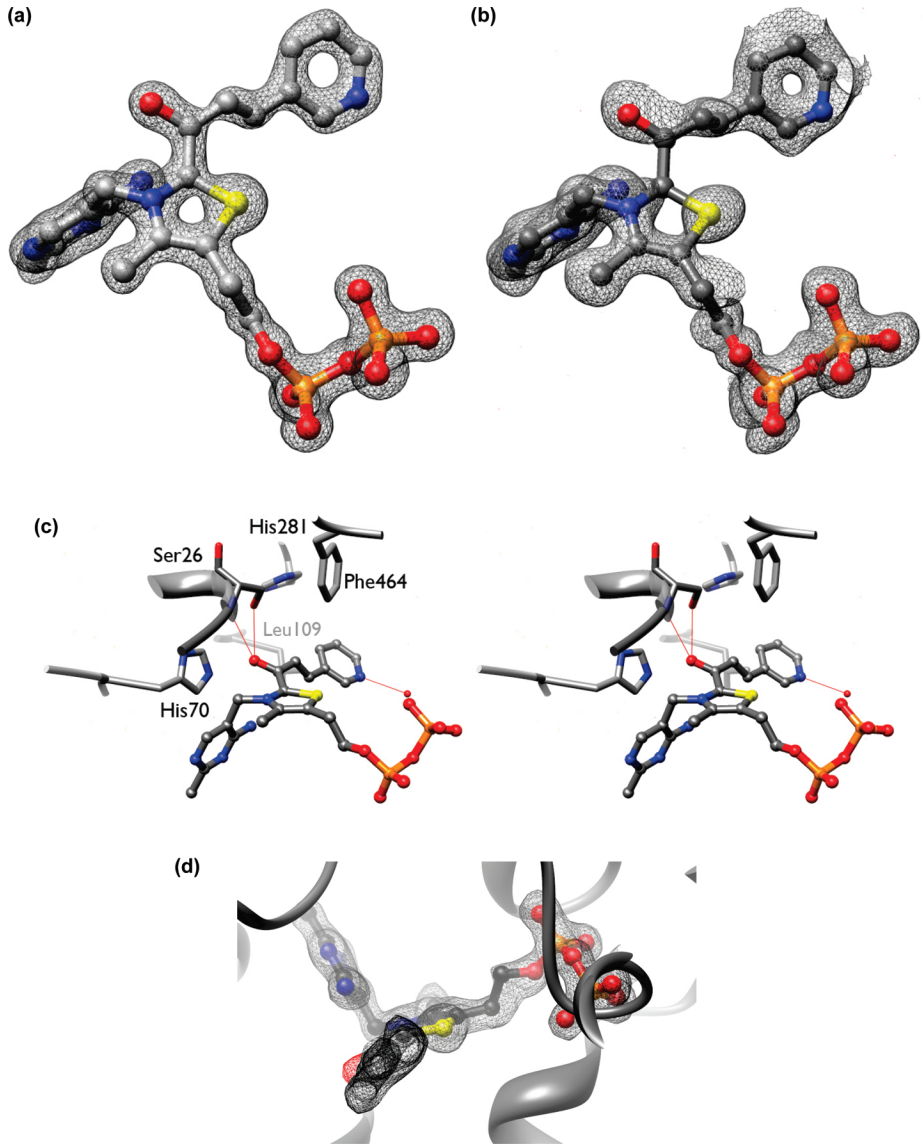

FIGURE 8: X-ray crystal structure of BFDC soaked with PAA (a) and 3-PKB (b) The gray mesh represents a $2F_o - F_c$ electron density map at the 1.5σ contour level. (c) Stereoview of residues contributing to stabilization of the PAA−ThDP adduct, showing likely hydrogen bonding network (red) and the positioning of catalytically important His70 and His281 side chains. (d) Electron density showing that the plane of the thiazolium ring (with sulfur atom in yellow) is not coplanar with the vinylpyridine (in black with nitrogen in blue). Also, note that the oxygen (electron density colored red) is out of the vinylpyridyl plane. The structures have been deposited as PDB entries 3F6B (for PAA) and 3F6E (for 3-PKB).

to this at 435 nm (*35*), indicating that the $C_6H_5CH{=}CH$ substituent at C2α will give a λ_{max} value in this immediate region with or without the ring nitrogen. In the absence of the CH=CH− group, the λ_{max} in models for the C_6H_5 substituent at C2α is ca. 380−385 nm. Thus, the assignment of T_2 to the enamine has strong support. While one could make an argument that the enamine could have two configurations, semiempirical calculations indicate that the same λ_{max} results for the two configurations of the enamine (data not shown). That is, the T_1 and T_2 could not simply be referring to different configurations of the enamine.

(d) Assignment of the 473 and 477 nm Transient Absorbances to the Tetrahedral Intermediates, PKB−ThDP and PHB−ThDP. The broad absorbances at λ_{max} 473 and 477 nm and their high extinction coefficients (*9*) suggest that they could correspond to a charge transfer (CT) transitions. Other than the enamine, there simply are no conjugated species in Scheme 2 that could have such a long wavelength λ_{max}. At the same time, we note that such CT bands involving ThDP have been identified: (a) the negative CD band at 320−330 nm that was attributed to ThDP on its cognate enzymes via a transition between the 4′-aminopyrimidine as donor and the thiazolium ring as acceptor (*17*); (b) our earlier studies on BFDC with *p*-nitrobenzoylformate (NBFA) as substrate also led to two transients with the first in time, T_1, appearing at 620 nm and the second in time, T_2, appearing at ca. 410 nm; the former was assigned to a predecarboxylation intermediate, the latter to the enamine (*7*).

The very broad bandwidth and large molar extinction coefficient of T_1 alerted us to the possibility that such intense bands could indeed represent covalent ThDP-bound intermediates.

Regarding the assignment of the T_1 transient derived from 3-PKB, several points are relevant. First, the transient intermediate T_1 at 477 nm appears before, and is depleted with the same rate as T_2 appears. Second, the same T_1 is produced from 3-PKB on three enzymes, YPDC (*9*−*11*), BAL (*32*) and BFDC (this study). Given the great variation in active centers, we believe that T_1 must correspond to the

same species on all three enzymes. Third, as shown in Figure 4, the same transient is produced from PAA (474 nm) and 3-PKB (477 nm), suggesting that the origin of the electronic transition is the same for the two. Since the spectral band produced from addition of PAA to BFDC is stable for longer time periods, it must pertain to a ThDP-bound covalent intermediate derived from the product, i.e., the PHB−ThDP. While this is a stable postdecarboxylation analogue, we believe that the 477 nm transient T_1 produced from 3-PKB, which is subsequently converted to the enamine T_2, *must correspond* to a predecarboxylation intermediate, either the Michaelis complex or the PKB−ThDP. The study of the PAA−ThDP adduct on BAL provided an additional bonus in that, on titration of BAL with PAA, we could observe simultaneous development of the negative CD band at 474 nm *and* of the positive CD band near 310−311 nm (Figure 6A). The latter has been attributed to the 1′,4′-imino tautomeric form of the species, which we observe *only* with tetrahedral substitution at C2α, but not with trigonal hybridization expected of the enamine. In other words, simultaneous observation of these two bands on BAL is only consistent with the presence of a tetrahedral adduct, such as PKB−ThDP or PHB−ThDP. On the basis of these experiments, assignment of T_2 to a predecarboxylation analogue is justified.

(e) Possible Source of the Electronic Transition Responsible for CT Band at 473 and 477 nm. If addition of either 3-PKB or PAA to BFDC produced intermediates with the same λ_{max} (within experimental error), this would strongly suggest that the same chromophore is responsible for the bands. Presumably these would correspond to the predecarboxylation and postdecarboxylation tetrahedral intermediates, but not the enamine, which has charge dispersal. We could suggest two possible alternatives for the CT band at 473 and 480 nm: (i) A CT transition resulting from an interaction between the pyridinyl group of 3-PKB as acceptor and the 1′,4′-iminopyrimidine ring of the PKB−ThDP as donor. The assignment to the 1′,4′-iminopyrimidine tautomer is based on evidence on six enzymes to date, indicating that, for the tetrahedral C2α substituent, this is the prevalent tautomeric form of the ThDP adduct (*14, 15, 17, 27*). Although we do not really know the pK_a of the pyridinium ring on the enzymes, the pK_a of the pyridinium ring of 3-PKB in solution is 4.3 (*9*), suggesting that, at the pH values used (6.0 or above on the three enzymes), the pyridine ring is in its conjugate base form. (ii) On the basis of a recent publication on a different ThDP enzyme which reported an enzyme-bound absorbance attributed to 2-acryloylThDP with a λ_{max} of 430 nm (*36*), we suggest a second alternative, in which the CT band at 473−477 nm is due to the interaction of the thiazolium ring as acceptor and the conjugated vinylpyridyl group of the adducts of 3-PKB or PAA with ThDP as donors. This certainly would be consistent with the fact that 3-PKB and PAA and their ThDP adducts share the same chromophore. This hypothesis is supported by models indicating that the vinylpyridyl chromophore is quite distant from the IP tautomer to be engaged in CT transitions. While the precise source of the CT transition is not yet known, the assignment to a pre- or post-decarboxylation tetrahedral ThDP adduct is sound.

(f) Observation of the True Enamine Derived from Benzaldehyde in BFDC. We could observe slow formation of the enamine near 383 nm when BFDC was reacted with the product benzaldehyde in the stopped-flow PDA instrument (Figure 7). Assignment of the transient with this wavelength was aided by our earlier model systems for this enamine, which gave an absorbance with λ_{max} at 380 nm (*5, 6*). This constitutes direct observation of the true enamine intermediate derived from a substrate or product on BFDC. The only species which could have an absorbance in this region is the enamine. Of the other potential candidates, benzoin absorbs at 314 nm, the 1′,4′-iminoThDP at 300−310 nm, and the aromatic rings could be ruled out.

(g) Evidence of "Alternating Active Site" Mechanism. Using the alternate substrate NBFA, it was proposed that BFDC, a homotetramer, behaves kinetically according to an "alternating active sites in a functional dimer" model (*7*). According to this model, the site in the second subunit of the dimer must be occupied by substrate before decarboxylation in the first site can be completed (*7*). With a conventional mechanism, the rate of decarboxylation of the PKB−ThDP (equivalent to the rate of enamine formation) should be independent of substrate concentration. As reported earlier for NBFA on BFDC (*7, 8*) and 3-PKB on YPDC (*9, 10*), this was not observed. Here it was again found that the rate constant for formation of both PKB−ThDP and the enamine increased with increasing 3-PKB concentration (Figure 2). Transient kinetic analysis of the concentration dependence of the two relaxations (Figure 2) enabled calculation of the K_d for both sites in the dimer. These differed substantially, with K_d values of 4.14 mM and 0.34 mM being obtained for the first and second sites, respectively. This behavior has now been observed on both YPDC and BFDC with two different conjugated substrate analogues. In fact, absent contrary experimental evidence, the concentration dependence of the rate of decarboxylation could be used as a signature for the alternating sites mechanism (*7, 8, 37*).

Additional evidence was obtained for the alternating active site mechanism when monitoring the progress curve for enamine formation from the true product benzaldehyde on BFDC (Figure 7). The results could be analyzed according to a model in which there are two active forms of the enzyme, the rate with the second one being nearly 5-fold larger than with the first one (reflected by a strong lag phase), again suggesting strong positive cooperativity with a slow transition between the two forms (Scheme 5).

(h) Electronic Structure and Chirality of the Enamine Intermediate. One of the fascinating observations of this study was the development of a positive CD signal in the stopped-flow CD experiments in the reaction between 3-PKB and BFDC at 435 nm. The electronic spectrum of the enamine intermediate confirms without any doubt that the intermediate is highly conjugated on the enzyme. Additionally, the enamine, being planar, is devoid of any chiral centers and thus should be achiral. Hence, the chirality must be induced on the enzyme.

(i) Structural Characterization of the Products of the Interaction of 3-PKB and PAA with BFDC. As can be seen in Figures 8a and 8b, both 3-PKB and PAA give rise to clear electron density in the vicinity of the ThDP cofactor. While the PAA−ThDP adduct is apparently covalent (Figure 8a), the electron density for the complex between 3-PKB and ThDP is less well defined (Figure 8b). The weak electron density observed between the S1 and C2 atoms of the

thiazolium ring in our view does not necessarily mean damage to the ring as observed in some X-ray structures of ThDP enzymes (*38*). A simulated annealing omit map shows that the peaks in the electron density are closer than the sum of the van der Waals radii of the two atoms, evidence for a chemical bond between S1 and C2. In fact, the ring electron density is observed to be continuous at any contour level below 1.3σ. One reason for the apparent weakness of the density between S1 and C2 may be that, even at fairly high spatial resolution, a signal 1−2 Å away from the S1 may be weakened by negative ripple from the sulfur atom. This Fourier series termination effect may artificially reduce the appearance of electron density between the two atoms (*39*).

A significant result deduced from the electron density of the PAA−ThDP adduct is that it clearly does not represent a planar, conjugated π system, such as the enamine that gives rise to the absorbance at 437 nm. Instead, the electron density reveals two planar systems, corresponding to the thiazolium ring and the vinylpyridine moiety (Figure 8d). In addition to the lack of overall planarity, the C2α carbon places its hydroxyl group out of either plane. All of these observations are consistent with assignment of this electron density to the PHB−ThDP species. However, the C2α chiral center appears considerably flattened from an ideal tetrahedron (Figure S2, Table S1 in the Supporting Information). This observation has some precedent in ThDP enzyme crystallography [branched chain keto acid decarboxylase (*40*), oxalylCoA decarboxylase (*41*), the E1 component of the pyruvate dehydrogenase complex from *Escherichia coli* (*42*), pyruvate oxidase (*43*), transketolase (*44*)]. The crystal structure of a small molecule analogue of HBThDP suggests some sp^2 character at the C2α position (*45*).

The reaction of BFDC with 3-PKB gives rise to a crystal structure that is similar overall to that seen with PAA. As shown in Figures 4, 5 and 8a, PAA reacts with ThDP to form a long-lived covalent adduct. Given that decarboxylation of 3-PKB produces PAA, the equilibrium state of BFDC treated with 3-PKB might be expected to be identical to that of enzyme treated with PAA. The fact that 3-PKB is rapidly decarboxylated leading to enamine formation on the stopped-flow time scale (Figure 1), is consistent with the structural finding that 3-PKB had undergone decarboxylation. Certainly, the electron density in Figure 8b does not seem to represent a complex between ThDP and 3-PKB as there is no evidence for the presence of the carboxylate. On the other hand, the evidence supporting a covalent PHB−ThDP complex is also weak, in view of the lack of electron density between C2α and C2 of the thiazolium ring. It may be that the observed electron density represents a mixture of species in the active site, or partial occupancy by the PHB−ThDP. Given the possibility of a mixture of species and strong evidence for the alternating sites mechanism, we were interested in the possibility of structural differences between active sites. The diffraction data were processed in a lower-symmetry space group (C_2), where the unit cell contains a protein dimer in the asymmetric unit, rather than the monomer seen in the I_{222} space group. Data processing in the absence of restraints for noncrystallographic symmetry allowed both active sites to be refined independently. Superposition of the two active sites revealed no significant differences between the two. The lack of electron density between the C2 and C2α atoms cannot be accounted for by differences among active sites within the tetramer. The bond angles and bond lengths deduced in Table S1 in the Supporting Information suggest that the structure of the 3-PKB−ThDP adduct is nearly the same as that of the PAA−ThDP adduct.

The residues involved in binding the covalent adduct of PAA and ThDP are shown in Figure 8c. As indicated, geometry and distance are favorable for the existence of hydrogen bonding interactions between the carbinol hydroxyl and the main chain and side chain of Ser26. Contacts that may be available to the pyridyl ring include a hydrogen bond to the nearby water, an edge−face interaction with Phe464, and a hydrophobic interaction with Leu109. Phe464 is an active site residue often seen to be disordered in BFDC structures (*1, 8*), but it is quite clear in the two structures reported here, suggesting the likelihood of stabilization through interaction with the pyridyl ring.

In summary, we have identified conditions for observation and characterization of the major covalent ThDP-bound intermediates (MThDP, HBThDP and enamine) in the catalytic cycle of the ThDP-dependent enzyme BFDC derived from substrate or substrate analogues. This is one of the rare instances where the product−ThDP covalent adduct is clearly observed, pointing to tetra-substituted C2α atom in the adduct according to both solution (CD spectroscopic) and solid state (X-ray crystallographic) evidence.

The high-resolution X-ray structure of the product−ThDP complex derived from the chromophoric substrate provided strong support for the visible spectral assignments to the various intermediates. It was also shown that the enamine does not exist in the IP form (hence must be in the AP or APH^+ forms), unlike in PHB−ThDP.

An especially intriguing fact is the chiral nature of the BFDC-bound enamine intermediate derived from the conjugated substrate analogue as reflected by the CD experiments. With the conjugated substrate analogue 3-PKB, *all of the intermediates in the catalytic cycle of BFDC could be observed by circular dichroism spectroscopy.*

The ability to directly observe the true enamine intermediate in BFDC using benzaldehyde as a substrate and the stability of this enamine intermediate for more than 5 min make this system a potential candidate for crystallization.

ACKNOWLEDGMENT

For Dr. Kenyon, this material was based on work supported by the NSF while he was working there. Any findings or conclusions expressed here are those of the author and do not necessarily reflect the views of the NSF.

SUPPORTING INFORMATION AVAILABLE

^{1}H NMR spectrum of the reaction mixture of BFDC and PAA after protein was removed by acid quench (Figure S1), bond distance and angle information on the PAA−ThDP adduct (Figure S2), and selected bond distances and bond angles from PAA-BFDC and 3-PKB-BFDC structures (Table

S1). This material is available free of charge via the Internet at http://pubs.acs.org.

REFERENCES

1. Hasson, M. S., Muscate, A., Mcleish, M. J., Polovnikova, L. S., Gerlt, J. A., Kenyon, G. L., Petsko, G. A., and Ringe, D. (1998) The Crystal Structure of Benzoylformate Decarboxylase at 1.6Å Resolution: Diversity of Catalytic Residues in Thiamin Diphosphate-Dependent Enzymes. *Biochemistry 37*, 9918–9930.
2. Weiss, P. M., Garcia, G. A., Kenyon, G. L., Cleland, W. W., and Cook, P. F. (1988) Kinetics and mechanism of benzoylformate decarboxylase using 13C and solvent deuterium isotope effects on benzoylformate and benzoylformate analogues. *Biochemistry 27*, 2197–2205.
3. Jordan, F. (2003) Current mechanistic understanding of thiamin diphosphate-dependent enzymatic reactions. *Nat. Prod. Rep. 20*, 184–201.
4. Jordan, F., and Nemeria, N. S. (2005) Experimental observation of thiamin diphosphate-bound intermediates on enzymes and mechanistic information derived from these observations. *Bioorg. Chem. 33*, 190–215.
5. Barletta, G., Huskey, W. P., and Jordan, F. (1992) Observation of a 2-α-enamine from a 2-[α-methoxy-α-phenyl]-3,4-dimethylthiazolium salt in water: Implications for catalysis by thiamin diphosphate -dependent α-keto acid decarboxylases. *J. Am. Chem. Soc. 114*, 7607–7608.
6. Barletta, G. L., Huskey, W. P., and Jordan, F. (1997) Ionization kinetics at the C2a position of 2- benzylthiazolium salts leading to enamines relevant to thiamin catalyzed enzymatic reactions. *J. Am. Chem. Soc. 119*, 2356–2362.
7. Sergienko, E. A., Wang, J., Polovnikova, L., Hasson, M. S., McLeish, M. J., Kenyon, G. L., and Jordan, F. (2000) Spectroscopic Detection of Transient Thiamin Diphosphate-Bound Intermediates on Benzoylformate Decarboxylase. *Biochemistry 39*, 13862–13869.
8. Polovnikova, E. S., McLeish, M. J., Sergienko, E. A., Burgner, J. T., Anderson, N. L., Bera, A. K., Jordan, F., Kenyon, G. L., and Hasson, M. S. (2003) Structural and Kinetic Analysis of Catalysis by Thiamin Diphosphate-Dependent Enzyme, Benzoylformate Decarboxylase. *Biochemistry 42*, 1820–1830.
9. Zhang, S. (2004) Ph.D. Dissertation, Department of Chemistry, Rutgers University, Newark, NJ.
10. Chakraborty, S. (2007) Ph.D. Dissertation, Department of Chemistry, Rutgers University, Newark, NJ.
11. Joseph E. (2005) Ph.D. Dissertation, Department of Chemistry, Rutgers University, Newark, NJ.
12. Jordan, F., and Mariam, Y. H. (1978) N-1′-Methyl thiamin, a model for the role of the pyrimidine ring in thiamin pyrophosphate requiring enzymatic reactions. *J. Am. Chem. Soc. 100*, 2534–2541.
13. Schellenberger, A. (1998) Sixty years of thiamin diphosphate biochemistry. *Biochim. Biophys. Acta 1385*, 177–186.
14. Nemeria, N., Chakraborty, S., Baykal, A., Korotchkina, L. G., Patel, M. S., and Jordan, F. (2007) The 1′,4′-iminopyrimidine tautomer of thiamin diphosphate is poised for catalysis in asymmetric active centers on enzymes. *Proc. Natl. Acad. Sci. U.S.A. 104*, 78–82.
15. Jordan, F., Zhang, Z., and Sergienko, E. (2002) Spectroscopic evidence for participation of the 1′,4′-imino tautomer of thiamin diphosphate in catalysis by yeast pyruvate decarboxylase. *Bioorg. Chem. 30*, 188–198.
16. Jordan, F., Nemeria, N. S., Zhang, S., Yan, Y., Arjunan, P., and Furey, W. (2003) Dual catalytic apparatus of the thiamin diphosphate coenzyme: acid-base via the 1′,4′-iminopyrimidine tautomer along with its electrophilic role. *J. Am. Chem. Soc. 125*, 12732–12738.
17. Nemeria, N., Baykal, A., Joseph, E., Zhang, S., Yan, Y., Furey, W., and Jordan, F. (2004) Tetrahedral intermediates in thiamin diphosphate-dependent decarboxylations exist as a 1′,4′-imino tautomeric form of the coenzyme, unlike the Michaelis complex or the free coenzyme. *Biochemistry 43*, 6565–6575.
18. Baykal, A. T., Kakalis, L., and Jordan, F. (2006) Electronic and nuclear magnetic resonance spectroscopic features of the 1′,4′-iminopyrimidine tautomeric form of thiamin diphosphate, a novel intermediate on enzymes requiring this coenzyme. *Biochemistry 45*, 7522–7528.
19. Nemeria, N., Korotchkina, L., McLeish, M. J., Kenyon, G. L., Patel, M. S., and Jordan, F. (2007) Elucidation of the chemistry of enzyme-bound thiamin diphosphate prior to substrate binding: Defining internal equilibria among tautomeric and ionization states. *Biochemistry 46*, 10739–10744.
20. Kale, S., Arjunan, P., Furey, W., and Jordan, F. (2007) A Dynamic Loop at the Active Center of the *Escherichia coli* Pyruvate Dehydrogenase Complex E1 Component Modulates Substrate Utilization and Chemical Communication with the E2 Component. *J. Biol. Chem. 282*, 28106–28116.
21. Nemeria, N. S., Korotchkina, L. G., Chakraborty, S., Patel, M., and Jordan, F. (2006) Acetylphosphinate is the most potent mechanism-based substrate-like inhibitor of both the human and *Escherichia coli* pyruvate dehydrogenase components of the pyruvate dehydrogenase complex. *Bioorg. Chem. 34*, 362–379.
22. Tittmann, K., Golbik, R., Uhlemann, K., Khailova, L., Schneider, G., Patel, M., Jordan, F., Chipman, D. M., Duggleby, R. G., and Hübner, G. (2003) NMR analysis of covalent intermediates in thiamin diphosphate enzymes. *Biochemistry 42*, 7885–7891.
23. Strell, M., and Kopp, E. (1958) Reactions in the pyridine series. II. Some reactions with pyridinealdehydes and cyanopyridines. *Chem. Ber. 91*, 1621–1631.
24. Iding, H., Dünnwald, T., Greiner, L., Liese, A., Müller, M., Siegert, P., Grötzinger, J., Demir, A. S., and Pohl, M. (2000) Benzoylformate decarboxylase from *Pseudomonas putida* as stable catalyst for the synthesis of chiral 2-hydroxyketones. *Chem.—Eur. J. 6*, 1483–1495.
25. Bradford, M. M. (1976) A rapid and sensitive method for the quantitation of microgram quantities of protein utilizing the principle of protein-dye binding. *Anal. Biochem. 72*, 248–254.
26. Yep, A., Kenyon, G. L., and McLeish, M. J. (2008) Saturation mutagenesis of putative catalytic residues of benzoylformate decarboxylase provides a challenge to the accepted mechanism. *Proc. Nat. Acad. Sci. U.S.A. 105*, 5733–5738.
27. Brandt, G. S., Nemeria, N., Chakraborty, S., McLeish, M. J., Yep, A., Kenyon, G. L., Petsko, G. A., Jordan, F., and Ringe, D. (2008) Probing the Active Center of Benzaldehyde Lyase with Substitutions and the Pseudosubstrate Analogue Benzoylphosphonic Acid Methyl Ester. *Biochemistry 47*, 7734–7743.
28. Kuo, D. J., and Jordan, F. (1983) Active Site Directed Irreversible Inactivation of Brewer's Yeast Pyruvate Decarboxylase by the Conjugated Substrate Analog 4(4-Chlorophenyl)-2-oxo-3-butenoic acid. *Biochemistry 22* 3735–3740.
29. Jordan, F., Adams, J., Farzami, B., and Kudzin, Z. H. (1986) Conjugated 2 Keto Acids as Mechanism- Based Inactivators of Brewer's Yeast Pyruvate Decarboxylase: Electronic Effects of Substituents and Detection of a Long-lived Intermediate". *J. Enzyme Inhib. 1*, 139–144.
30. Annan, N., Paris, R., and Jordan, F. (1989) p-Halomethylbenzylidene pyruvic acids inactivate yeast pyruvate decarboxylase by a variety of mechanisms. *J. Am. Chem. Soc. 111*, 8895–8901.
31. Zeng, X. (1992) Ph.D. Dissertation, Rutgers University, Graduate Faculty at Newark.
32. Chakraborty, S., Nemeria, N., Yep, A., McLeish, M. J., Kenyon, G. L., and Jordan, F. (2008) Mechanism of Benzaldehyde Lyase Studied via Thiamin Diphosphate-Bound Intermediates and Kinetic Isotope Effects. *Biochemistry 47*, 3800–3809.
33. Bernasconi, C. F. (1976) *Relaxation Kinetics*, pp 24−25, Academic Press, New York, San Francisco, London.
34. Zhang, S., Zhou, L., Nemeria, N., Yan, Y., Zhang, Z., Zou, Y., and Jordan, F. (2005) Evidence for Dramatic Acceleration of a C-H Bond Ionization Rate in Thiamin Diphosphate Enzymes by the Protein Environment. *Biochemistry 44*, 2237–2243.
35. Zeng, X., Chung, A., Haran, M., and Jordan, F. (1991) Direct Observation of the Kinetic Fate of a ThDP bound Enamine Intermediate on Brewers' Yeast Pyruvate Decarboxylase. *J. Am. Chem. Soc. 113*, 5842–5849.
36. Merski, M., and Townsend, C. A. (2007) Observation of an acryloyl-thiamin diphosphate adduct in the first step of clavulanic acid biosynthesis. *J. Am. Chem. Soc. 129*, 15750–15751.
37. Sergienko, E. A., and Jordan, F. (2002) New Model for Activation of Yeast Pyruvate Decarboxylase by Substrate Consistent with the Alternating Sites Mechanism: Demonstration of the Existence of Two Active Forms of the Enzyme. *Biochemistry 41*, 3952–3967.
38. Dobritzsch, D., König, S., Schneider, G., and Lu, G. (1998) High resolution crystal structure of pyruvate decarboxylase from *Zymomonas mobilis*. *J. Biol. Chem. 273*, 20196–20204.
39. Einsle, O., Tezcan, F. A., Andrade, S. L., Schmid, B., Yoshida, M., Howard, J. B., and Rees, D. C. (2002) Nitrogenase MoFe-protein at 1.16 Å resolution: a central ligand in the FeMo-cofactor. *Science 297*, 1696–1700.

40. Berthold, C. L., Gocke, D., Wood, M. D., Leeper, F. J., Pohl, M., and Schneider, G. (2007) Structure of the branched-chain keto acid decarboxylase (KdcA) from *Lactococcus lactis* provides insights into the structural basis for the chemoselective and enantioselective carboligation reaction. *Acta Crystallogr. D63*, 1217–1224.

41. Berthold, C. L., Toyota, C. G., Moussatche, P., Wood, M. D., Leeper, F., Richards, N. G., and Lindqvist, Y. (2007) Crystallographic snapshots of oxalyl-CoA decarboxylase give insights into catalysis by nonoxidative ThDP-dependent decarboxylases. *Structure 15*, 853–861.

42. Arjunan, P., Sax, M., Brunskill, A., Chandrasekhar, K., Nemeria, N., Zhang, S., Jordan, F., and Furey, W. (2006) A thiamin-bound, pre-decarboxylation reaction intermediate analogue in the pyruvate dehydrogenase E1 subunit induces large scale disorder-to-order transformations in the enzyme and reveals novel structural features in the covalently bound adduct. *J. Biol. Chem. 281*, 15296–15303.

43. Wille, G., Meyer, D., Steinmetz, A., Hinze, E., Golbik, R., and Tittmann, K. (2006) The catalytic cycle of a thiamin diphosphate enzyme examined by cryocrystallography. *Nat. Chem. Biol. 2*, 324–328.

44. Asztalos, P., Parthier, C., Golbik, R., Kleinschmidt, M., Hübner, G., Weiss, M. S., Friedemann, R., Wille, G., and Tittmann, K. (2007) Strain and near attack conformers in enzymic thiamin catalysis: X-ray crystallographic snapshots of bacterial transketolase in covalent complex with donor ketoses xylulose 5-phosphate and fructose 6-phosphate, and in noncovalent complex with acceptor aldose ribose 5-phosphate. *Biochemistry 46*, 12037–12052.

45. Turano, A., Furey, W., Pletcher, J., Sax, M., Pike, D., and Kluger, R. (1982) Synthesis and crystal-structure of an analog of 2-(alpha-lactyl)thiamin, racemic methyl 2-hydroxy-2-(2-thiamin)ethylphosphonate chloride trihydrate - a conformation for a least-motion, maximum-overlap mechanism for thiamin catalysis. *J. Am. Chem. Soc. 104*, 3089–3095.

BI801810H